Proceedings of the
International Conference on Mechanical Engineering and Renewable Energy 2019
(ICMERE2019) 11 – 13 December, 2019, Chittagong, Bangladesh

ICMERE2019-PI-053

NUMERICAL INVESTIGATION OF FLOW FIELDS FOR DAWT'S DIFFUSER MODEL WITH DIFFERENT FLANGE ANGLES

A.S.M. Rokonuzzaman[1], **Md. Golam Kader**[1] **and Maksudul Alam**[1]
[1]Department of Mechanical Engineering,
Khulna University of Engineering & Technology, Khulna 9203, Bangladesh
rokonuzzamanbasit96@gmail.com*, mdgolamkader@gmail.com, maksudulalam.kuet.me@gmail.com

***Abstract*-** *The idea of Diffuser Augmented Wind Turbine has been adopted for several years to produce more power from wind turbine from same wind velocity. Diffuser helps to create more velocity inside it and leads to obtain more power. Flange at the end of the diffuser can create low pressure behind the diffuser resulting in more flow velocity of wind through the diffuser thus enhancing diffuser performance. In this work, an axisymmetric two dimensional flanged diffuser has been numerically investigated for different flange angle. The flange angle varied from +25° to -25° with vertical at interval of 5°. The flange angled with +15° downstream has shown more velocity at the entrance of the diffuser (45.26%) than the other flanged diffuser. Various flow properties such as velocity magnitude, static pressure and pressure coefficients along different sections of the diffuser have been discussed.*

Keywords: Diffuser Augmented Wind Turbine, Flanged Diffuser, CFD

1. INTRODUCTION

The continuous improvement of the world is dependent on the advancement of technology, which is directly related to utilization of energy. Since the demand of energy is creeping up every day, sources of conventional energy are becoming limited resulting in making them more expensive [1]. As the improvement and utilization of sustainable, clean energy have turned into a vital issue in recent years because of the genuine impacts of a global temperature rise and quick consumption of non-renewable energy sources, different methods for elective energy sources are being assessed to face the present situation of energy emergency. Among all of the renewable energy solar, hydraulic and wind power are the most common energy forms which can generate power that meets a huge portion of world's energy demand.

Wind is a natural, clean source of energy. The nation's wind supply is abundant, inexhaustible and sustainable. If power of wind can be utilized efficiently to produce power it has the potential of influence in resolving the power demand of the entire world. Wind turbine is a device that converts kinetic energy of wind into mechanical energy which later used for production of electrical energy. There are two main types of wind turbine: (HAWT) horizontal axis wind turbine and (VAWT) vertical axis wind turbine [2].

Diffuser augmented wind turbine is one of the most popular concepts of wind power augmented systems where a traditional horizontal axis wind turbine is surrounded by a cone shaped diffuser. Due to the wind turbine being enclosed by the diffuser, the pressure will drop behind the turbine. As a result, velocity of wind approaching the turbine increases. Thus, the diffuser provides increased wind velocity i.e. increased wind energy density to the wind turbine [3].

Wind power generation in wind turbine is directly proportional to the cube of served wind speed. Therefore, if it is possible to create even a slight increase in the velocity of the impending wind to a wind turbine, a large increase in output can be obtained. The speed of available wind is increased in DAWT with the help of diffuser to create high power output. The low static pressure results in increased mass flow through the turbine rotor compared to a conventional turbine of the same diameter.

Foreman et al. [4] investigated an experiment on DAWT which resulted in twice power intensity compared to the traditional wind turbine. Hansen et al. [5] investigated on the CFD calculations of an exposed turbine with the hypothetical articulation for the power coefficient. Abe and Ohya [6] examined the flow fields around a flanged DAWT utilizing CFD for a wind turbines under 1.5 kW. Abe et al. [7] numerically and practically experimented for stream fields of a little wind turbine with a flanged diffuser. Shives and Crawford [8] numerically experimented combined blade-element, CFD model for the prediction of performance and optimization of ducted turbines. Göltenbott et al. used DAWT for multi rotor system where aerodynamics of two and three DAWTs were experimented in a wind tunnel. The rotors were spaced in close vicinity in same plane and have been organized [9].

2. AERODYNAMICS OF DIFFUSER

The geometry of diffuser for DAWT is such that the cross sectional area of the diffuser with respect to its axis is increasing continuously towards downstream direction. The wind turbine will be placed at the entrance of the diffuser where the cross sectional area is the lowest. As a result, wind flow rate approaching the wind turbine will increased. The flange helps to create the low pressure region behind the diffuser, which results in more wind flow through the diffuser.

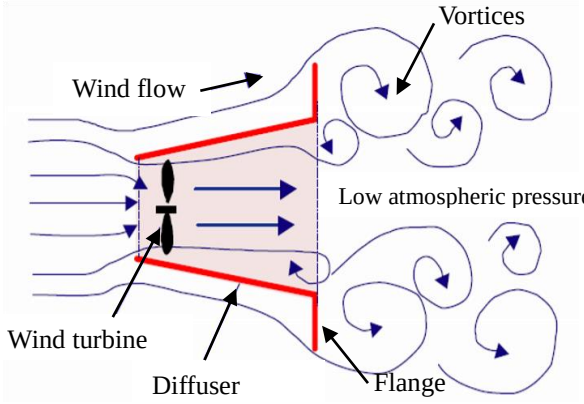

Fig.1: Schematic cross sectional view of diffuser augmented wind turbine

Continuity, momentum, and energy are the governing equations that can describe the present problem configuration. For the present problem, air is taken as a working medium whereas the flow is assumed to be steady, turbulent, incompressible and two-dimensional. M. El-Zahaby et al. [10] assumed standard K-ε model, a common method that employs the Boussinesq hypothesis to relate the Reynolds stresses to the mean velocity gradient.

$$-\rho u_i u_j = \mu\left[\frac{\partial u_i}{\partial x_j}+\frac{\partial u_j}{\partial u_i}\right]-\frac{2}{3}\left[\rho K+\frac{\partial u_i}{\partial x_j}\right]\delta_{ij} \quad (1)$$

μ is the dynamic viscosity of the fluid, and $u_i\, u_j$ is the turbulent Reynolds stress. After modeling the Reynolds stresses term the above governing equations can be simplified as follows:

Continuity Equation:

$$\frac{\partial(\rho u)}{\partial x}+\frac{\partial(\rho v)}{\partial y}=0 \quad (2)$$

Momentum Equations:
x – Direction:

$$\frac{\partial(\rho u^2)}{\partial x}+\frac{\partial(\rho uv)}{\partial y}=-\frac{\partial p}{\partial x}+\frac{\partial}{\partial x}\left[\mu_e\frac{\partial u}{\partial x}\right]+\frac{\partial}{\partial y}\left[\mu_e\frac{\partial u}{\partial y}\right]-\frac{2}{3}\frac{\partial}{\partial x}(\rho K)+\rho g_x \quad (3)$$

y – Direction:

$$\frac{\partial(\rho uv)}{\partial x}+\frac{\partial(\rho v^2)}{\partial y}=-\frac{\partial P}{\partial y}+\frac{\partial}{\partial x}\left[\mu_e\frac{\partial v}{\partial x}\right]+\frac{\partial}{\partial y}\left[\mu_e\frac{\partial v}{\partial y}\right]-\frac{2}{3}\frac{\partial}{\partial y}(\rho K) \quad (4)$$

Where, μ is the effective viscosity.

Turbulence Equation
K–Equation:

$$\frac{\partial(\rho uK)}{\partial x}+\frac{\partial(\rho vK)}{\partial y}=\frac{\partial}{\partial y}+\frac{\partial}{\partial x}\left[\left(\mu+\frac{\mu_t}{\sigma_k}\right)\frac{\partial K}{\partial x}\right]+\frac{\partial}{\partial y}\left[\left(\mu+\frac{\mu_t}{\sigma_k}\right)+\frac{\partial K}{\partial y}\right]-g\frac{\mu_t}{\mathrm{Pr}_t}\frac{\partial P}{\partial x}+\mu_t\left\{2\left(\frac{\partial\mu}{\partial x}\right)^2+\left(\frac{\partial v}{\partial y}\right)^2+\left(\frac{\partial\mu}{\partial x}+\frac{\partial v}{\partial y}\right)^2\right\}-\rho\varepsilon \quad (5)$$

ε–Equation:

$$\frac{\partial(\rho u\varepsilon)}{\partial x}+\frac{\partial(\rho v\varepsilon)}{\partial y}=\frac{\partial}{\partial x}\left[\left(\mu+\frac{\mu_t}{\sigma_\varepsilon}\right)\frac{\partial\varepsilon}{\partial x}\right]+\frac{\partial}{\partial y}\left[\left(\mu+\frac{\mu_t}{\sigma_\varepsilon}\right)+\frac{\partial\varepsilon}{\partial y}\right]-C_{1\varepsilon}\frac{\varepsilon}{K}g\frac{\mu_t}{\mathrm{Pr}_t}\frac{\partial P}{\partial x}+C_{1\varepsilon}\frac{\varepsilon}{K}\mu_t\left\{2\left(\frac{\partial\mu}{\partial x}\right)^2+\left(\frac{\partial v}{\partial y}\right)^2+\left(\frac{\partial\mu}{\partial x}+\frac{\partial v}{\partial y}\right)^2\right\}-C_{2\varepsilon}\rho\frac{\varepsilon^2}{K} \quad (6)$$

3. METHODOLOGY

Preprocessing and post processing are two important steps in achieving CFD solution. Preprocessing steps consists of mesh generation followed by converting the mesh into a CFD solver solvable format. Post processing involves visualization of obtained results done by post processing software which is often coupled with CFD solver.

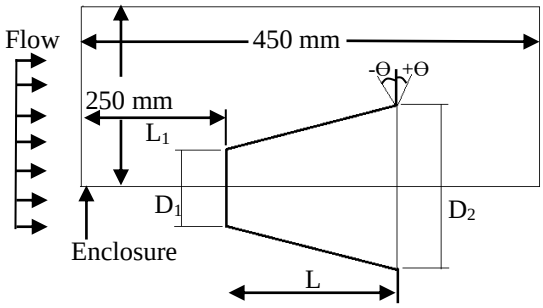

Fig.2: Schematic of diffuser models

3.1 Geometry Drawing

Geometry of a two dimensional diffuser was modeled in 'Design Modular Geometry' of CFD solver ANSYS Fluent. As the diffuser is symmetric to any plane across the length of the diffuser, the geometry can be taken as axisymmetric. Figure 3 shows the two dimensional axisymmetric geometry profile of the diffuser with flange angle 15° clockwise (downstream).

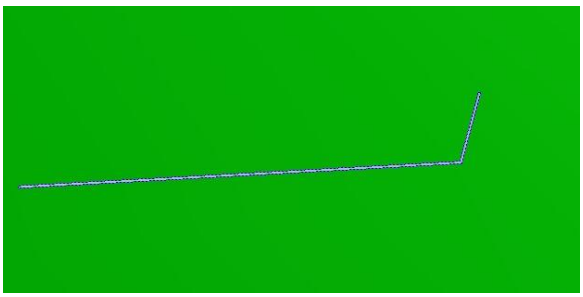

Fig.3: Diffuser with a flange angle 15° clockwise

In total, 11 geometries of diffuser were modeled where the flange of the diffuser varies from Θ= -25 degree to Θ=+25 degree by 5 degree intervals. The various dimensions of the diffuser models were the following: diffuser inlet diameter, D_1=0.120 m, diffuser outlet diameter, D_2=0.140 m, length of the diffuser, L= 180 mm, flange height 30 mm. The total enclosure of the system was taken as a rectangle of 450 mm in length and 250 mm in width. The free stream length which is the length from the left wall (from where the flow is coming) to the diffuser entrance (denoted in fig.2 as 'L_1') was kept 120 mm. The downside wall coincides with the axis of the diffuser with respect to which the diffuser is symmetrical.

3.2 Mesh Generation

Generated mesh is shown in the following figure where fig.4 shows mesh generated in the two dimensional axisymmetric system of the diffuser.

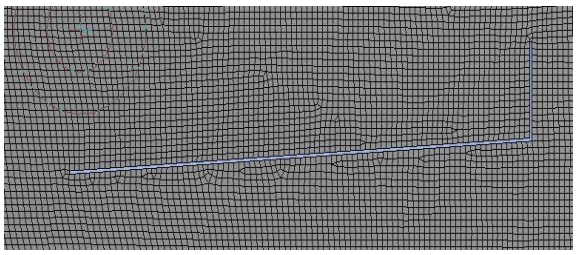

Fig.4: Generated mesh with flange angle 0°

Left wall of the enclosure is the inlet, from where the air flow will go through the diffuser. Upper wall of the enclosure is the far-field and the lower one is the symmetric line for the system. Total number of nodes were 115000-116000 for different diffuser geometries.

3.3 Solver Settings

As from the assumptions of the actuator disk theory of wind turbine, the flow is steady. The solver was set with viscous flow, standard K-ε equation with standard wall function. Pressure based with absolute velocity formulation was set to solve the problem. No slip conditions were maintained in all of the stationary walls.

3.4 Boundary Conditions

The boundary conditions in the inlet wall and outlet wall were defined by fixing the wind speed at the inlet. SIMPLE (Semi-Implicit Method for Pressure Linked equations) and SIMPLEC (Semi-Implicit Method for Pressure Linked Equations-Consistent) methods were evaluated for different operative conditions. The residual values for all of the parameter (continuity, x-velocity, y-velocity and k) were set as 10^{-5}. That means the simulation process was considered to be converged when the residuals decrease under 10^{-5}.

Table 1: Boundary Condition for diffuser

Parameters	Boundary Conditions
Inlet velocity Magnitude	4.5 m/s
Initial gauge Pressure	101325 Pascal
Turbulent Intensity	5%
Turbulent Viscosity Ratio	10
Outlet Gauge Pressure	0 Pascal
Wall roughness height	0 m
Wall roughness constant	0.5

3.5 Mesh Independency

It's important to make sure that the calculated results don't vary with different mesh settings and create confusion. For that, different meshing was done to solve the system of the diffuser. Four different meshing was done and calculated followed by finding the wind velocity at the diffuser entrance. Table 2 shows the number of nodes with corresponding wind velocity at diffuser entrance for flange angle 0°. Area weighted average velocity was measured here for this purpose.

Table 2: Data for mesh independency test

Serial no.	No. of Nodes	Entrance Velocity (m/s)
1	78393	6.496866
2	93854	6.298534
3	115709	6.476793
4	143512	6.476715

Figure 5 elaborates the process showing velocity at diffuser entrance for different meshing. It can be noticed that diffuser entrance velocity is same for meshing where total no. of node is 115709 and 143512. So it can be said that meshing 3 which have 115709 nodes can be chosen as ideal domain for calculation.

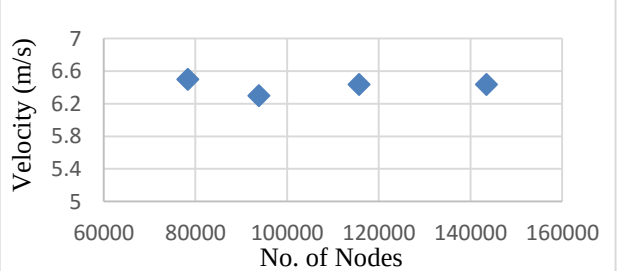

Fig.5: Mesh Independency for different meshing

3.6 Validation

The present study of the model is validated with the study of Abe et al. [7], where a flanged diffuser were numerically investigated along with which experimental research were also done. Numerically obtained results were compared with their experimental data. Figure 6 shows the comparison of the experimental result with present results.

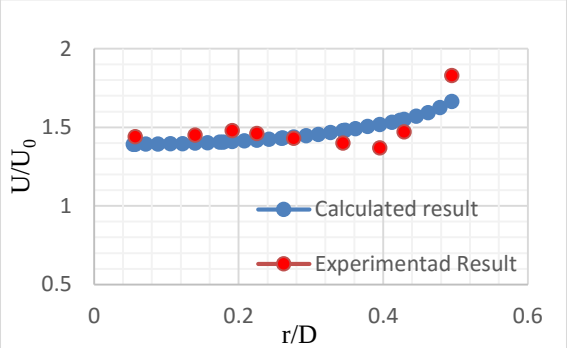

Fig.6: Validation of present study with experimented results

In the graph, the abscissa represents the radial distance from axis of the diffuser towards the diffuser wall. The y-axis represents the velocity increase i.e. the ratio of wind velocity at diffuser entrance to free stream wind velocity.

4. Result and Discussion

11 diffuser geometries were studied and numerically investigated. Different flow properties such as velocity distribution, pressure distribution and pressure coefficients were studied.

4.1 Velocity Profiles

The simulation was done for different flange angles of diffuser varies from -25 degree to +25 degree and variation of velocity in the domain was observed. Velocity contour for flange angle 0° is shown on the following figure, where velocity at the inlet wall is 4.5 m/s. Here, all the velocities are in unit of m/s.

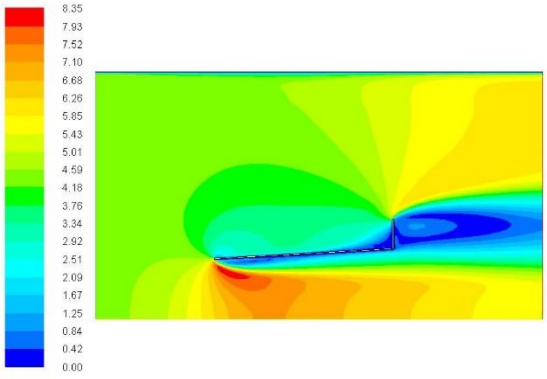

Fig.7: Velocity contour for flange angle 0°

From fig.7 the velocity profile of wind flow through the diffuser can be observed. Wind flow comes at velocity 4.5 m/s from the left wall which is the inlet wall of the system. The velocity is noticed to rise inside the diffuser after entering in to it. The formation of boundary layer can also be observed on inside of diffuser wall. As 'no slip' condition was applied on the diffuser wall, air velocity adjacent to diffuser wall is zero.

4.2 Pressure Profile

Variation of pressure was observed just like velocity. Figure 8 shows profile of pressure of the system for inlet velocity 4.5 m/s for flange angle 0°. Here, pressure distribution has been shown in Pascal or N/m^2.

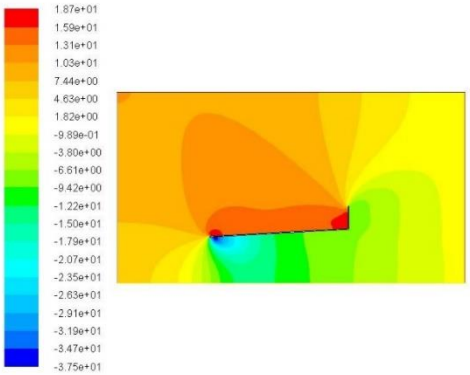

Fig.8: Pressure contour for flange angle 0°

It is noticeable that at the entrance of the diffuser, the pressure falls. The function of flange with a diffuser is also clear as pressure falls after the flange area which leads to more air forced through the diffuser and ultimately resulting the increased velocity at the diffuser entrance.

4.3 Effect of Flange Angle

To observe the effect of flange angle on wind velocity at diffuser entrance, a line at diffuser entrance starting from the symmetry line to diffuser wall was taken and area weighed velocity was measured.

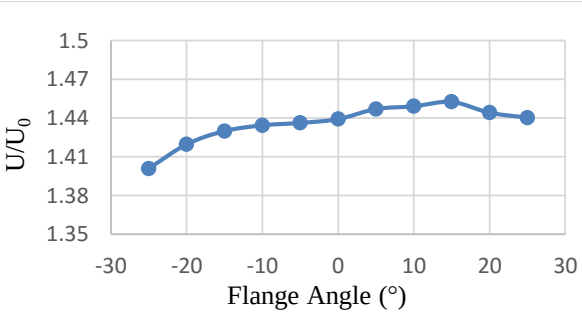

Fig.9: Velocity Increase for different flange angle at Diffuser Inlet

It can be observed that the average velocity increase at diffuser entrance is highest for flange angle 15°. The velocity increase i.e. ratio of wind velocity at diffuser entrance to free stream wind velocity gets lower behind flange angle 0°, keeps rising at positive flange angles up to 15°. After flange angle +15°, values of U/U_0 tend to get lower again.

The magnitude of wind velocity at diffuser entrance for flange angle 15° is 6.537 m/s, where the free stream velocity of wind was 4.5 m/s. From the data of fig.9, for 15° flange angle, the value of U/U_0 is 1.45263 which means velocity has increased 45.263% of original wind velocity.

4.4 Velocity Distribution through the diffuser

The radius of the diffuser was taken as 60 millimeter for calculations. Now, to show the variation of air velocity at different radius of the diffuser along its length, several horizontal lines were drawn in the post processing step. Each line were 10 millimeter vertically apart from each other.

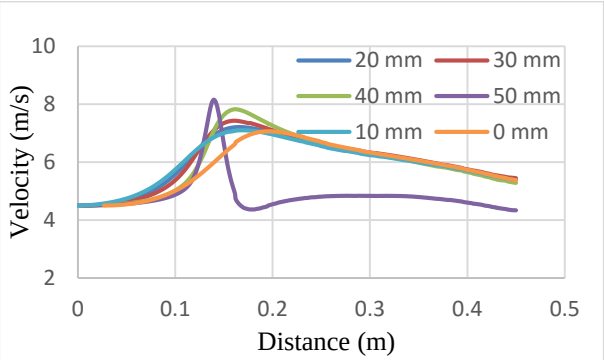

Fig.10: Velocity for flange angle15°

Figure 10 contains velocity distributions along the length of the system for flange angle 15° where the diffuser entrance is at 120 mm distance from the inlet wall. From the figure it can be noticed that the velocity of air rises at this entrances. As the line y=50 mm is closest of these lines to diffuser wall, velocity along this line rises up faster than other lines and also falls down due to viscous effect of air and boundary layer formation.

As the line showing velocity at 50 mm radial distance is dramatically different from the other lines, to further understand the nature of the variation of velocity of wind through diffuser, more studies were done about the velocity distribution near the diffuser walls. This time, data were taken for every 2 mm radial distance to understand the gradual change of wind velocity

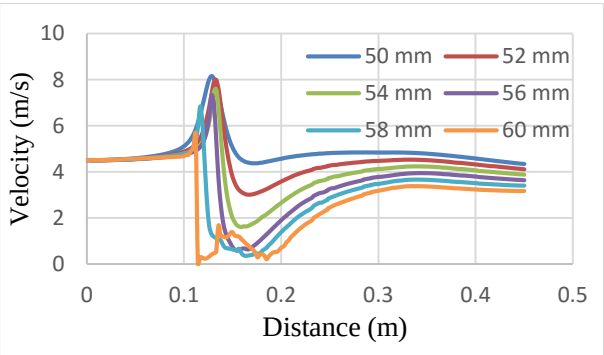

Fig.11: Wind velocity near diffuser wall

Figure 11 shows variation of velocity along horizontal lines that passes close and through the diffuser. It is noticeable that the velocities are changing gradually at diffuser entrance section. It can be observed that velocity at 60 mm radial distance drops to complete zero as the proof of "no slip condition" at diffuser wall. As a result of boundary layer formation, velocity magnitudes are decreasing as the lines are getting closer to the diffuser wall.

To visualize the velocity distribution more properly, surface plot have been made showing velocity at both flow direction and radial direction of diffuser.

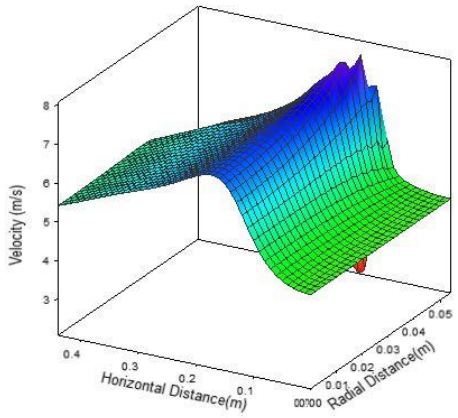

Fig.12: Velocity variation in different direction

Figure 12 and 13 represents the surface plot showing the variation of velocity through the diffuser with flange angle 15°. From fig.12, it is noticeable that the velocity increases along the length of the system (y axis) while the x axis represents the radial distance of the diffuser.

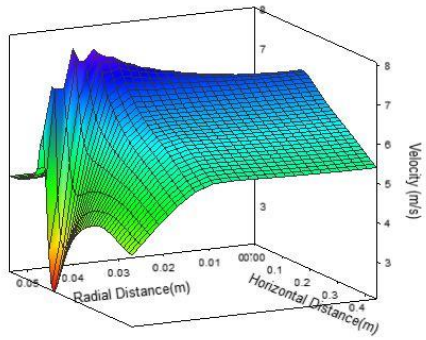

Fig.13: Velocity variation in different direction

It can be observed from fig.13 that the velocity drops down after radial distance 56 mm which is due to formation of boundary layer and no slip condition at diffuser wall surface.

4.5 Pressure distribution through the Diffuser

Static pressure variation along the drawn horizontal lines have been shown here in the following fig.14. It is noticeable that the static pressure falls down at the entrance of the diffuser which is at 0.120 m distance on this graph due to velocity rise i.e. rise of dynamic pressure.

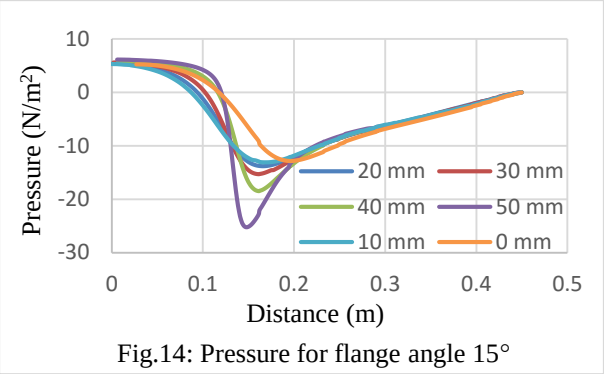

Fig.14: Pressure for flange angle 15°

It is noticeable that the line representing pressure variation at 50 mm line is distinctive than the others. The pressure at this level falls dramatically compared to others because this line is closer to diffuser wall (which is at 60 mm radius at its entrance), due to which pressure has effect from boundary layer as velocity at this level were also noticed to be unusual than other lines.

4.6 Variation of Pressure Coefficient

Pressure produced from wind turbine is related with the pressure drop of wind by passing through the turbine rotor. Pressure coefficient indicates the pressure drop as well as the effectiveness of the wind turbine to produce power.

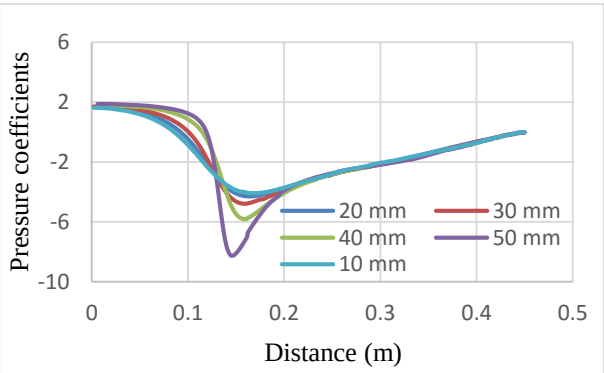

Fig.15: Pressure coefficients for 15°

Figure 15 shows the variation pressure coefficient along the horizontal lines through the diffuser. As pressure coefficient is a dimensionless number and independent of body size, an actual large diffuser can be analyzed with same pressure coefficients.

5. CONCLUSION

An axisymmetric two dimensional diffuser was modeled in design modular geometry of CFD solver ANSYS Fluent. Eleven different geometries were made with different flange angle of diffuser and their effect on velocity at diffuser entrance have been analyzed. It has been found that diffuser with flange angle 15 degree with vertical to downstream gives highest air velocity at diffuser entrance which is 45.263% of the free stream velocity and 3% more power output than diffuser with flange angle 0°. Various flow properties (velocity magnitude, static pressure, pressure coefficient) of the flow passing through the diffuser have been analyzed. At the entrance of the diffuser, flow tends to have more velocity towards the center of the diffuser. Wind velocity is relatively low at the region near to the diffuser wall due to the boundary layer formation. Pressure coefficients varies along with static pressure. Static pressure is independent of body size, so it can be applied to analyze large sized diffuser.

6. REFERENCES

[1] Benchmarking of Biodiesel Fuel Standardization in East Asia Working Group (2010), 'Energy Situation in the World' in Goto, S., M. Oguma, and N. Chollacoop, EAS-ERIA Biodiesel Fuel Trade Handbook: 2010, Jakarta: ERIA, pp.6-15.

[2] J.H. Strickland, "The Darrieus Turbine: a performance model using multiple stream tube." 1975. SAND 75-0431.

[3] T. Saravana Kannan, Saad A. Mutasher, Y.H. Kenny Lau, "Design and Flow Velocity Simulation Of Diffuser Augmented Wind Turbine Using Cfd." Journal of Engineering Science and Technology Vol. 8, No. 4 (2013) 372 – 384

[4] Foreman, B. Gilbert, R.A. Oman, "Diffuser augmentation of wind turbines." Sol. Energy 20 (1978).

[5] M.O.L. Hansen, N.N. Sorensen, R.G.J. Flay," Effect of placing a diffuser around a wind turbine." J. Fluid Mech. 3 (2000) 207–213

[6] K. Abe, Y. Ohya, "An investigation of flow fields around flanged diffusers using CFD." J. Wind Eng. Ind. Aerodyn. 92 (2004) 315– 330

[7] K. Abe, M. Nishida, M.A. Sakurai, Y. Ohya, H. Kihara, E. Wada, K. Sato, "Experimental and numerical investigations of flow fields behind a small-type wind turbine with flanged diffuser." J. Wind Eng. Ind. Aerodyn. 93 (2005) 951-970

[8] Michael Shives and Curran Crawford, "Ducted Turbine Blade Optimization Using Numerical Simulation." ISBN 978-1-880653-96-8

[9] U Göltenbott, Y Ohya, S Yoshida and P Jamieson "Flow interaction of diffuser augmented wind turbines." doi:10.1088/1742-6596/753/2/022038

[10] M. El-Zahaby, A.E. Kabeel , S.S. Elsayed, M.F. Obiaa, "CFD analysis is of flow fields for shrouded wind turbine's diffuser model with different flange angles." Alexandria Engineering Journal (2017) 56, 171–179

7. NOMENCLATURE

Symbol	Meaning	Unit
D1	Diameter of diffuser's inlet	m
D2	Diameter of diffuser's Outlet	m
L	Diffuser Length	m
U0	Free stream wind speed Mean wind speed	m/s
U	Mean wind speed through diffuser	m/s
Θ	Flange angle	°